scientific reports

Check for updates

OPEN

Mechanisms and control of large deformation in mudstone roof gob side entry of inclined coal seams with water softening

Chunyang Tian[1,2], Jingchen Chang[1], Zijian Li[1], Dongdong Chen[1]✉, Shikun Xing[3], Zhixuan Zhang[1], Wenkang Zhao[1] & Xiangyu Yang[1]

The gob-side entry in the inclined coal seams of the Songxinzhuang Coal Mine faces severe deformation under the influence of mudstone roofs water immersion-softened, and the conventional support is invalid. The main conclusions are as follows: (1) This study, through laboratory experiments both the macroscopic (water immersion tests) and microscopic (XRD and SEM) perspectives, reveals that the strength and bearing capacity of the mudstone in the immediate roof will reduce after water immersion softening, which is the root cause of the large deformation of the roadway from. (2) Through theoretical analysis established a stability evaluation system based on the softened friction angle (φ') and the sliding stability coefficient (K_1), and results showing that the key roof blocks above the gob-side entry become unstable under water-softened conditions. (3) Through simulations reveal the stress field distribution and evolution patterns of the surrounding rock under mudstone water immersion conditions. And results indicate that the mudstone under water-softened intensifies the expansion and coalescence of stress peak zones. When the softening depth exceeds 6–8 m, stress concentrations at the right rib increase rapidly and spread toward the roof and floor, forming a "stress envelope". (4) Based on these findings, an asymmetric support strategy integrating grouting and drainage with a combined roof-bolt and steel-beam system was proposed. This approach effectively mitigates the impact of water immersion and enhances roadway stability. Field monitoring validated the effectiveness of this support system in controlling deformation and maintaining the integrity of the surrounding rock, providing critical guidance for managing similar challenges in inclined coal seams.

Keywords Inclined coal seam, Mudstone water immersion, Surrounding rock control, Gob-side entry

In China, coal has always been the primary energy source for the development of the national economy, and the Ningdong mining area, as a large coal base of China's billion tons, plays a crucial role in the national supply of energy[1]. Ningdong mining area has its typical resource occurrence conditions: (1) The overlying pseudo-roof of the coal seam has many bedding structures, and the direct roof contains a large number of clay minerals that swell and soften with water, resulting in low strength[2,3]; (2) The basic roof is thick sandstone with a hard texture. Once the working face is mined, the roof of the goaf is suspended and the mining roadway pressure is significant[4–6]; (3) Coal seam mining causes mining and primary cracks to propagate. Groundwater in saturated areas, combined with goaf water accumulation, weakens the lower working face and its immediate roof. Increased roadway pressure during working face mining raises support costs and threatens subsequent production and replacement work[7–9]. In particular, with the mining of coal seams with better occurrence conditions, asymmetric severe large deformation occurs along the empty roadway driving complex and difficult-to-mine inclined working faces due to unbalanced loading and groundwater inrush weakening the strength of surrounding rock.

Researchers both domestically and internationally have conducted extensive studies on the movement patterns of overlying strata in inclined coal seams, especially in steeply inclined coal seams, the monitoring and prevention technology of geological disasters, the control principle and technology of roadway surrounding rock support and the mechanism of water-rock coupling. The research on the migration law of overlying strata in inclined coal seams is as follows: Currently, there have been a series of changes and breakthroughs

[1]School of Energy and Mining Engineering, China University of Mining and Technology-Beijing, Beijing 100083, China. [2]Songxinzhuang Coal Mine, Qingyang, China. [3]Jizhong Energy Co., Ltd. Xingdong Mine, Xingtai, China. ✉email: 18796246989@163.com

in fully mechanized mining technology for extracting steeply inclined coal seams in China, including control of surrounding rock, equipment efficiency, and stability management[10]; Steeply inclined coal seam mining and overburden rock migration[11]; Stress and displacement changes in overlying strata of steeply inclined coal seams affected by faults[12]; Impact of inclined coal seam mining on surface subsidence[13–16]; Using gangue and grouting filling to control inclined coal seam goaf[17–20]; Research on geological disaster monitoring and prevention technology: References[21,22] implemented real-time monitoring of rockbursts in steeply inclined coal seams, enabling timely warnings, and proposed principles for rockburst prevention and load reduction; Pressure relief technologies related to preventing high-energy distortion zones of rockbursts during the mining of deep, steeply inclined coal seams[23]; Control principle and technical research of roadway surrounding rock support: estimation method and failure mechanism of coal pillar strength in inclined coal seam[24–26]; Scheme for managing large deformation support in inclined coal seam gob-side entry[27]; Deep buried steeply inclined roadway support[28]; Pre-splitting blasting method for alleviating pressure in the hard roof of inclined faces[29]; Research and development of inclined coal seam roadway surrounding rock deformation, stress monitoring new technology[30]. Research on water-rock coupling: This study[31] explores the degradation of mechanical properties in coal rock samples with different crack widths after varying soaking times; Influence of ground water inrush from goaf of steeply inclined coal seam on surface deformation[32]; The influence metrics of water flow in fractured zones during comprehensive mechanized mining of coal seams beneath water bodies[33]; Literature[34] detailed the analysis of fracture field evolution in coal and rock masses over time and space through numerical simulations and a digital ray scanning mechanical testing system; The development of mining-induced fissures in weathered bedrock under the action of high-pressure water-sand flow[35]; Roof water inrush mechanism and prevention under different mining sequences in karst mining area[36]. It provides mechanical and theoretical basis for the mechanism analysis of coal mine spalling rockburst, and helps to optimize the early warning and prevention and control measures of dynamic disasters (such as roof pre-splitting, coal pressure relief, etc.)[37].

In conclusion, researchers both domestically and internationally have made significant advancements in the economic, safe, and efficient extraction of inclined coal seam working faces. Nevertheless, there is a deficiency of systematic and standardized research regarding the mechanical properties of surrounding rock, the migration of hinged structures in overlying rock, and the support control of roadway surrounding rock under the combined influence of aquifer groundwater and water in goaf. Therefore, this paper takes the return airway of 110,304 working face in Songxinzhuang Coal Mine (large deformation roadway affected by water immersion) as the research object, and analyzes the stress and stability of the hinged structure of overlying strata in gob-side entry under the influence of water immersion by means of comprehensive research methods such as "real-time field monitoring + laboratory test + theoretical calculation + physical similarity simulation experiment + numerical simulation experiment". The asymmetric failure mechanism and stress field evolution characteristics of surrounding rock of gob-side entry and overlying immediate roof under the influence of different water immersion weakening degree and water immersion range are controlled and analyzed. The asymmetric large deformation support control technology of "grouting drainage + shed cable joint" is proposed. Practice has proved that the research has important reference significance for the support control of water-immersed roadway under similar working conditions.

Project overview and large deformation issues of the roadway

Geological overview of the roadway

This research project is located at the Song Xinzhuang coal mine, with the main mining areas including the adjacent 110,302 and 110,304 working faces. Figure 1 shows the study area's geologic information. The coal seam layers are steeply inclined at an angle of 20°. The main coal seam being mined is the 3# coal seam, with an average thickness of 2 m and a burial depth of 320 m. A 16-meter-wide protective coal pillar is preserved between the 110,302 transportation roadway and the 110,304 return airway. The direct roof of the coal seam is mudstone(3.2 m); it is easily weathered and has poor resistance to water immersion. The overlying strata consist

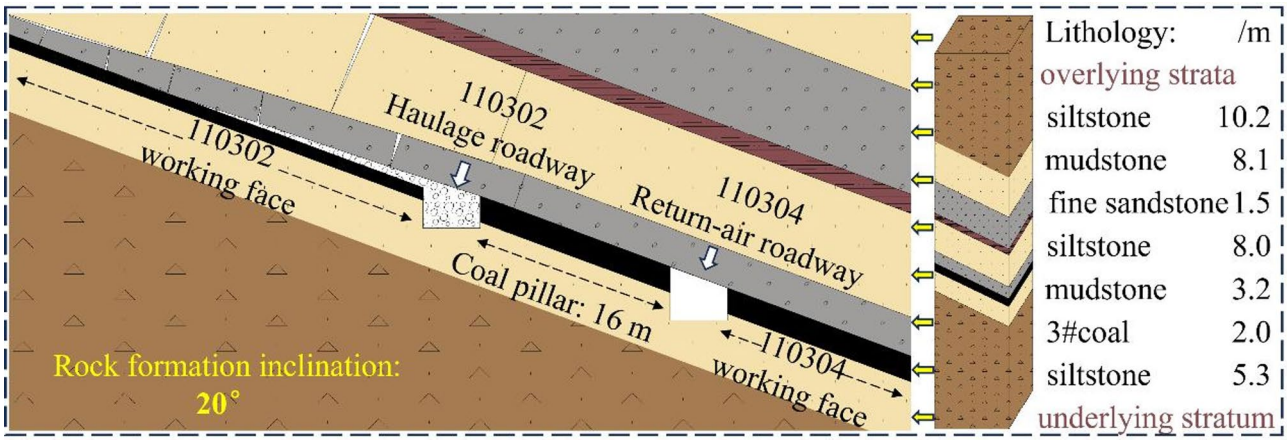

Fig. 1. Geological information of the mining area.

of an 8-meter-thick siltstone, which is water-bearing and relatively hard. The direct floor consists of siltstone with an average thickness of 5.3 m. The 110,302 working face(110302WF) has been mined out, and the next step is to proceed with the mining of the 110,304 working face (110304WF). The goaf is prone to water accumulation and accumulates in the coal pillar area on the side of the goaf. Water has a weakening effect on the coal pillar and the mudstone above the coal pillar, especially on the mudstone.

Characteristics of large deformation in the roadway

Engineering challenges

During the mining of the 110302WF, the roadways in the mining area experienced severe deformation, frequent roof collapses, and floor heaving. Effective support could not be applied, as shown in Fig. 2. After significant deformation occurred, some cross-sections of the roadway had an actual height of less than 0.8 m, which severely impacted the access of equipment and personnel, as well as the extraction of resources from the mine. This also posed a serious safety threat to the workers.

Preliminary analysis of large deformation of roadways

The on-site exploration data show that the 110302WF of the 3# coal seam has water from the pore fissures of the roof sandstone and water from the wind-oxidized zone as water sources. Moreover, there are fully developed weathering fissures between the 110302WF and the upper aquifer, and the two have obvious hydraulic connections. And the mining fissures of the 110302WF provide a water filling channel.

During the excavation stage of the 110302WF, its water inflow continued to increase, and the coal pillars and their roof and floor plates were infiltrated. The research team initially analyzed that the cause of tunnel damage was that the strength of the coal rock mass was reduced after infiltration, the bearing capacity was insufficient, and even some areas failed, resulting in uncontrollable large deformation of the mining area roadways. The selected geological conditions and mining technology of Songxinzhuang Coal Mine are typical, and the research results can provide reference for similar mining areas.

Experimental study on the load-bearing failure characteristics of coal and rock under water immersion

Water immersion test of coal and rock mass

Samples were taken from the direct roof mudstone, coal pillar, and main roof sandstone within the mining area, and cylindrical specimens of identical size were prepared (diameter × height: 50 × 25 mm) for laboratory water immersion experiments. Each of the three types of specimens, differing only in lithology, was placed in a transparent container and immersed in room-temperature water. The containers were then promptly placed in a digital constant-temperature water bath set to an ambient temperature of 25 °C. The integrity and disintegration degree of each specimen were observed and recorded after identical immersion durations.

As shown in Fig. 3, all three rock samples exhibited good integrity prior to immersion. However, after short-term immersion (5 min, 30 min), the mudstone softened and disintegrated much faster than the coal and siltstone samples. With extended immersion time, this difference became increasingly pronounced. Compared to the siltstone sample, the coal sample released bubbles on its surface during immersion, with the number of bubbles first increasing and then decreasing over time. This is mainly due to the gradual filling of micro-pores and fractures within the coal sample by water. The siltstone sample remained the most stable during immersion, with no significant change in integrity or visible bubble release on its surface, indicating low permeability.

The coal and rock sampling tests revealed that the direct roof mudstone in the mining area has a marked tendency to soften upon water exposure. According to the hydrogeological report, the area is in a water-immersed environment after mining operations are suspended. Combined with the water immersion test, it was found that the integrity of the direct roof mudstone is severely compromised under water immersion, while the siltstone of the main roof and direct floor remains largely unaffected. This finding is also consistent with what is shown in Fig. 3.

The above water immersion tests provide a macroscopic view of the softening and damage characteristics of different rock samples under immersion. To precisely analyze the causes of large deformation, SEM (scanning electron microscopy) and XRD (X-ray diffraction) tests were conducted on the same batch of samples from the water immersion tests to analyze the object phase composition and microstructure of the samples.

Analysis of XRD diffraction results

The mineral compositions of two groups of mudstone samples were analyzed that using a X-ray diffractometer.

As shown in Fig. 4, the X-ray diffraction patterns of two mudstone samples. The samples included in the test are divided into two different groups: A-1 sample and A-2 sample. The two groups of samples mainly contain three minerals: quartz, kaolinite and chlorite.

The X-ray diffraction patterns of mudstone samples were semi-quantitatively analyzed by JADE 9.0 software, and the relative contents of three main minerals were obtained. Among them, Quartz has the highest content, accounting for approximately half of the relative content of the three minerals, and it exhibits highly stable physical and chemical properties. Followed by Kaolinite, which makes up approximately 30% of the relative content of the three minerals. Kaolinite undergoes a certain degree of volume expansion when it absorbs water, leading to the disintegration of mudstone. Chlorite has a relatively lower content, accounting for roughly 20% of the relative content of the three minerals, and its properties are relatively stable.

The chlorite and kaolinite detected in the mudstone samples are all clay minerals. Based on the above analysis results, apart from the stable quartz, clay minerals are the main components of mudstone. The two samples are both rich in clay minerals, and the strength of these minerals will decrease significantly once they come into

Fig. 2. Large deformation of the roadway in the mining area.

contact with water. Therefore, the unique nature of mudstone rock minerals dominated by clay minerals is the root cause of its low strength and poor bearing capacity.

Analysis of SEM scanning electron microscope experimental results

To conduct an in-depth analysis of the internal microstructure of dried mudstones, an SEM scanning experiment was performed using a Hitachi SU8010 electron microscope on experimental rock samples. Specifically, two sets of dried mudstones, labeled as A-1 and A-2, were scanned at magnifications of 1000 times, 2000 times, and 5000 times. The experimental results are shown in Fig. 5.

The experimental results indicate:

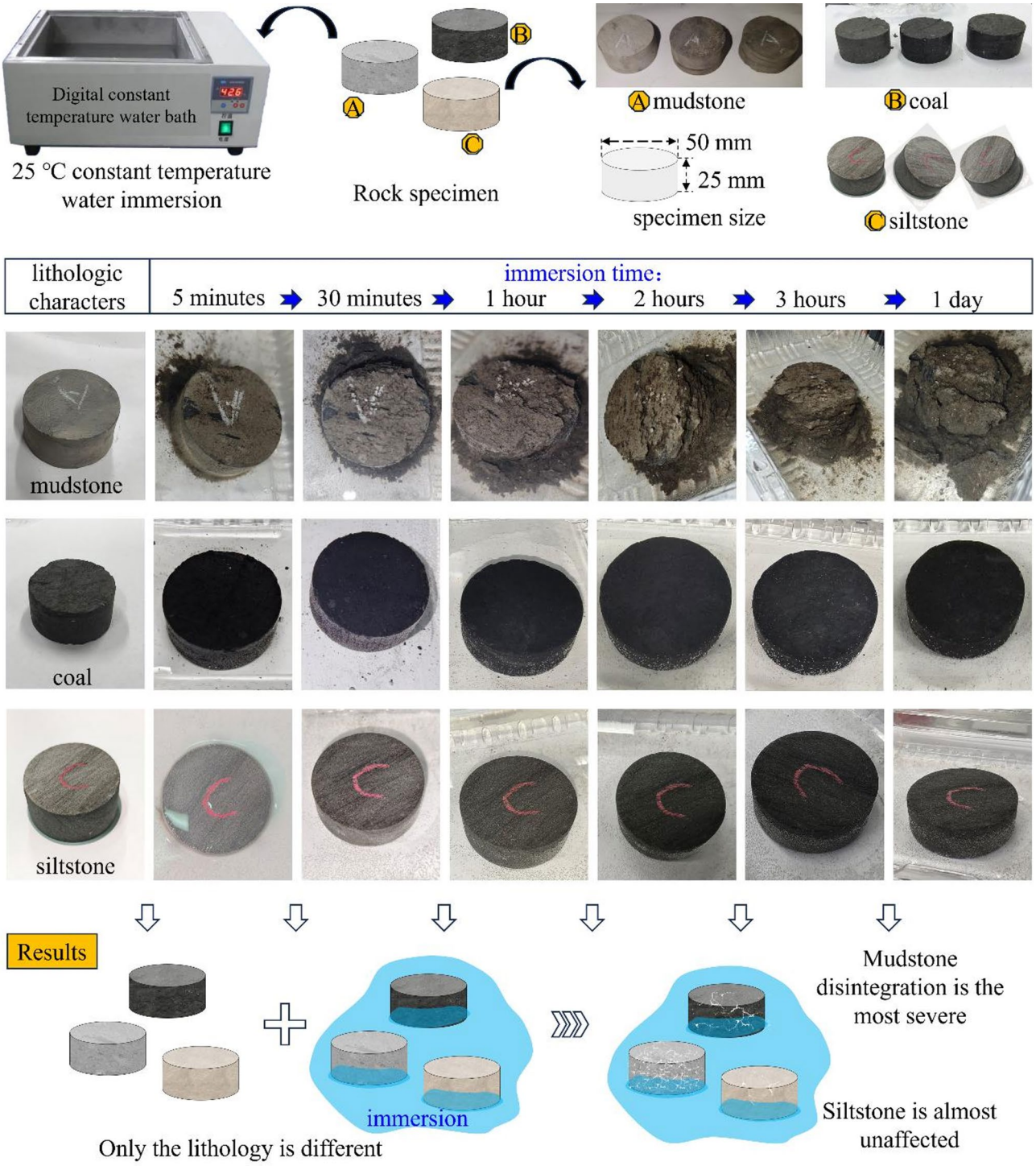

Fig. 3. Degree of influence of water immersion on rock samples with different lithologies in the mining area.

(1) In its natural state, the rock sample is primarily composed of quartz, kaolinite, chlorite, and other minerals distributed in the form of particles. It has a relatively smooth overall appearance and a high degree of structural integrity.
(2) When the rock sample is magnified 1000 times, quartz is widely distributed, and pores between particle units within the rock sample become visible. The overall structure of both mudstone samples is no longer smooth.
(3) When the rock sample is magnified 2000 times, interlaced cracks appear in locally separated block areas.
(4) When the rock sample is magnified 5000 times, kaolinite particles distributed within the rock sample in its natural state mostly exhibit a lamellar (or platelet-like) structure.

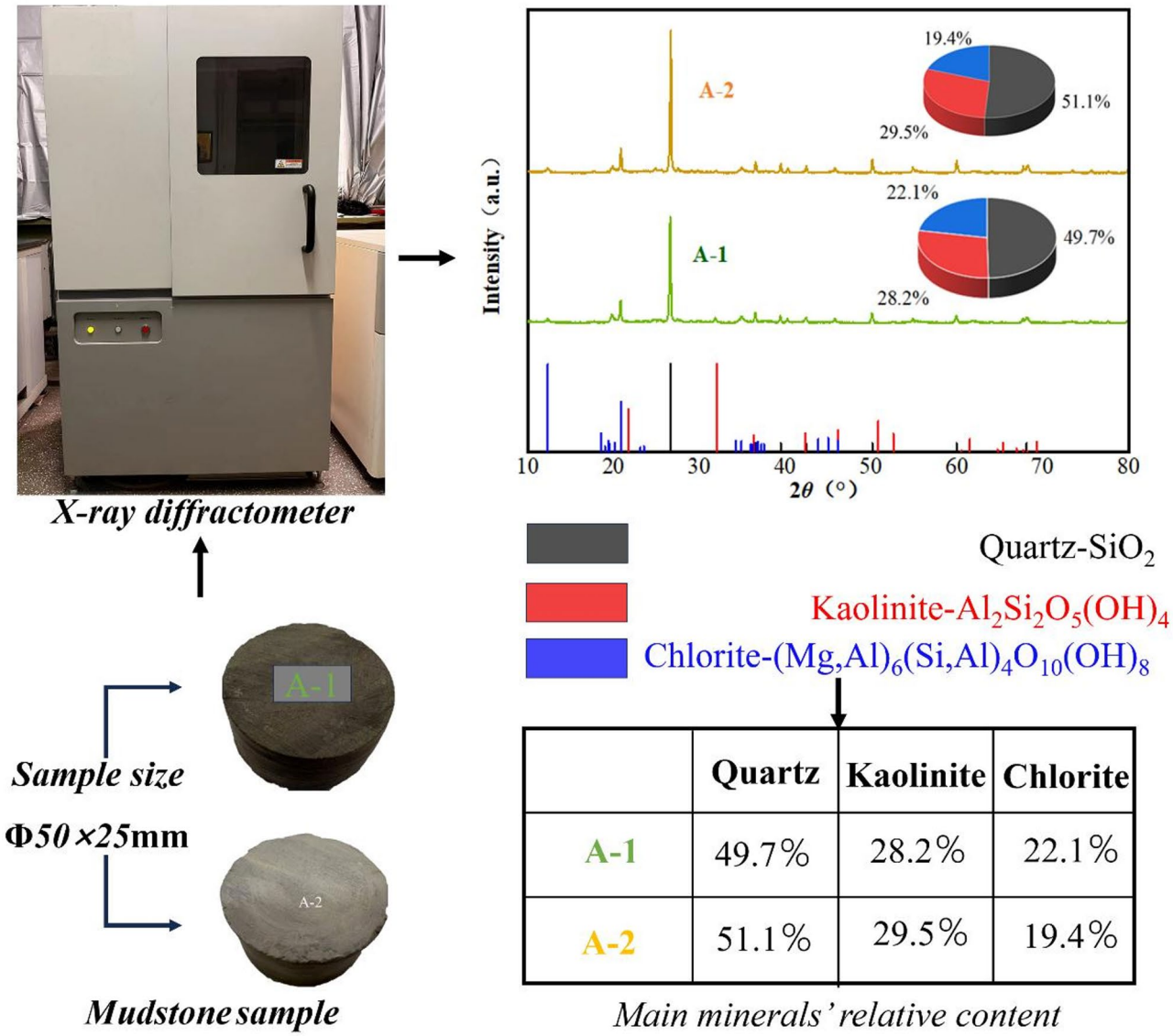

Fig. 4. X-ray diffraction pattern of mudstone samples.

After soaking and damaging the two groups of mudstone samples, electron microscope scanning experiments were conducted again at magnifications of 1000 times, 2000 times, and 5000 times, respectively. The experimental results are shown in Fig. 6.

The experimental results indicate:

(1) In their natural state, both groups of mudstone samples disintegrate and turn into mud after being soaked in water, resulting in a significant drop in their strength.
(2) When the rock sample is magnified 1000 times, large pores become clearly visible.
(3) When the rock sample is magnified 2000 times, the extreme unevenness of its surface becomes even more apparent.
(4) When the rock sample is magnified 5000 times, adjacent pores interconnect to form larger pores, leading to block separation within the sample.

Mechanical analysis of the failure mechanism of the overlying strata roof under water immersion

Considering that the main roof is immersed in water, after simplifying the critical triangular block structure, the stress diagram shown in Figs. 7 and 8 is established by CAD 2024.

When moments of all forces are taken about the rotation axis *LL'*, the resultant moment is zero.

$$\sum M_{LL'} = 0 \tag{1}$$

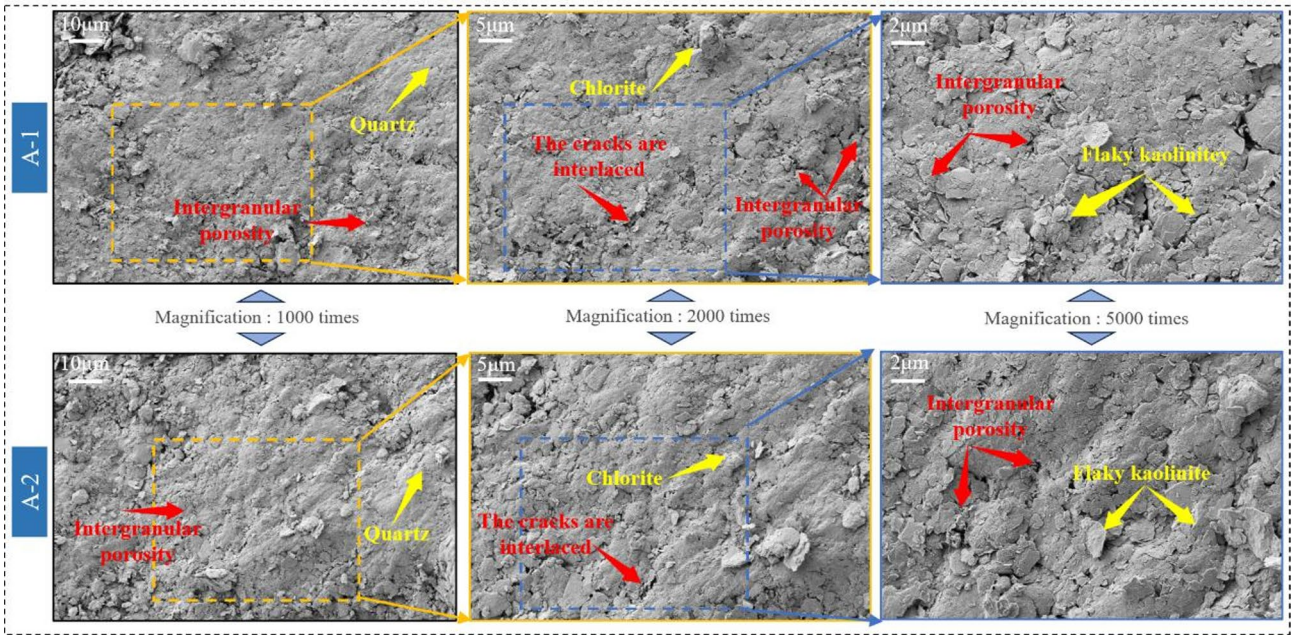

Fig. 5. SEM scanning results of dried mudstone.

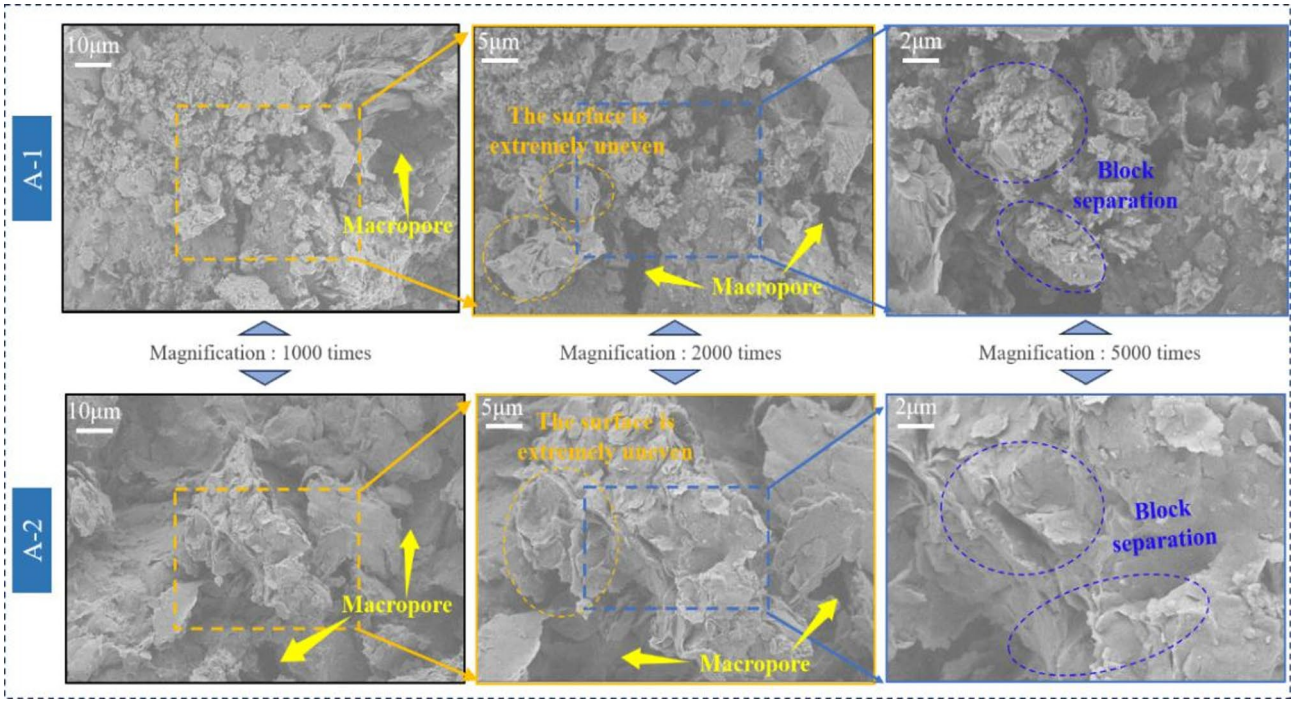

Fig. 6. The electron microscope scanning result of water-immersed mudstone.

$$2T_{BC}a\cos\alpha + \int_{0}^{x_0} f_M\left[\frac{-2}{\tan\alpha}(x-L_2)\right]xdx + \int_{x_0}^{L_2\cos\theta} f_g\left[\frac{-2}{\tan\alpha}(x-L_2)\right]xdx$$
$$-2R_{CB}\cos\theta\frac{L_2}{2} - (F_R+F_Z)\cos\theta\frac{L_2}{3} = 0 \quad (2)$$

Where f_g represents supporting force of gangue per unit area, f_M represents supporting force of coal body per unit area.

Solve R_{CB}:

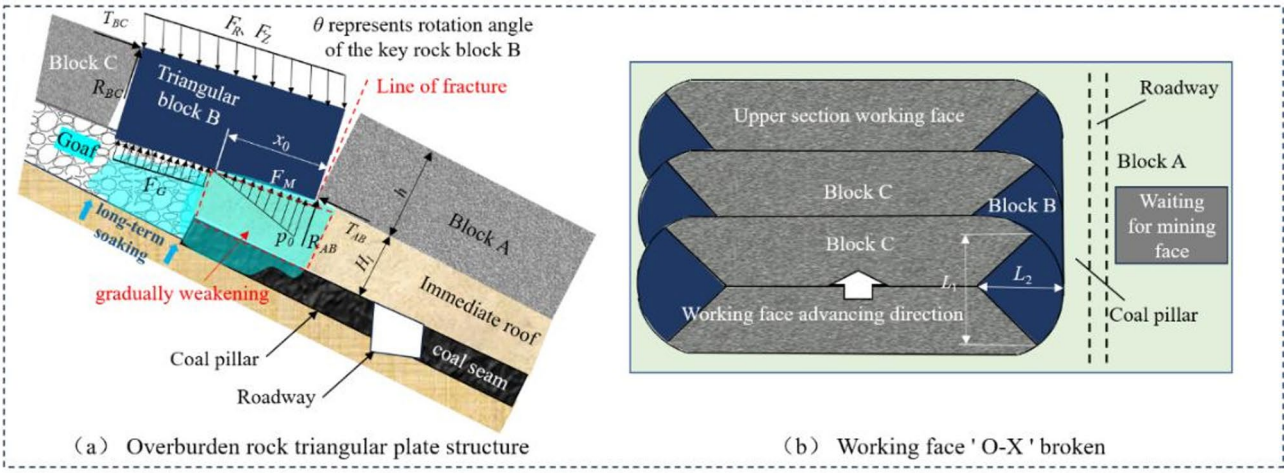

Fig. 7. Triangular block structure of overlying rock along goaf side.

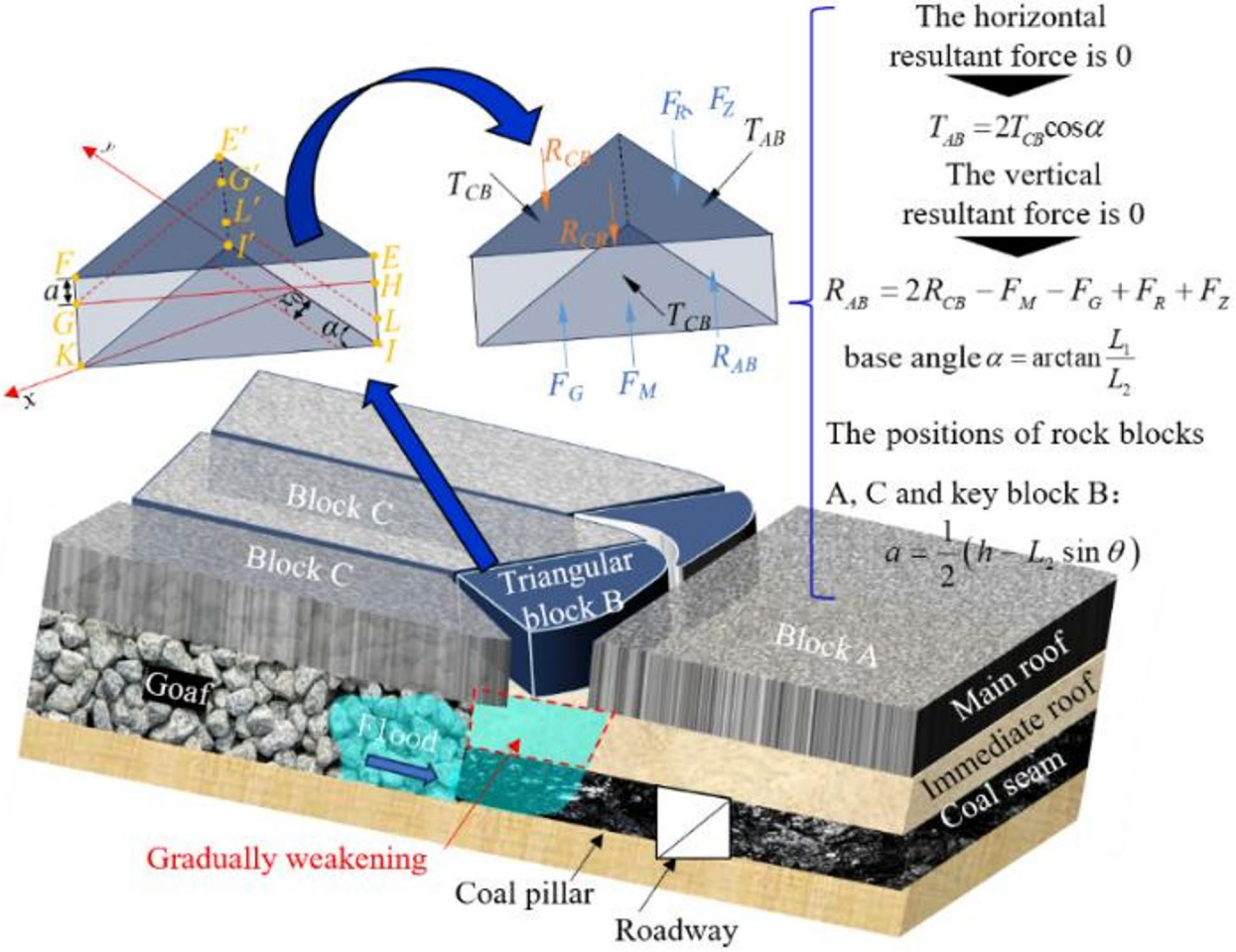

Fig. 8. Three-dimensional model of key triangular block structure.

$$R_{CB} = \frac{1}{L_2 \cos\theta}\left\{2T_{CB}a\cos\alpha + \int_0^{x_0} f_M \frac{-2}{\tan\alpha}(x - L_2)\,xdx + \int_{x_0}^{L_2\cos\theta} f_g \frac{-2}{\tan\alpha}(x - L_2)\,xdx - \frac{L_2}{3}(F_Z + F_R)\cos\theta\right\} \tag{3}$$

$$T_{CB} = \frac{L_2(F_R + F_Z)}{2\left(h - \frac{L_2\sin\theta}{2}\right)}. \tag{4}$$

Where F_R represents self-weight of rock block B, F_Z represents resultant force of the self-weight of the overlying rock strata.

Under the effect of water immersion weakening, the supporting force F_M of the coal body below the triangular block B on the arcuate triangular block is calculated using the following formula:

$$F_M = \int_0^{x_0} f_M \left[\frac{-2}{\tan\alpha}(x - L_2)\right] dx. \tag{5}$$

Supporting force of the caved gangue F_G:

$$F_G = \int_{x_0}^{L_2\cos\theta} f_g \left[\frac{-2}{\tan\alpha}(x - L_2)\right] dx. \tag{6}$$

The solution to R_{AB} can be obtained:

$$\begin{aligned} R_{AB} = {} & \frac{4aT_{CB}\cos\alpha}{L_2\cos\theta} + \frac{-4f_M}{L_2\cos\theta\tan\alpha}\left(\frac{1}{3}x_0^3 - \frac{1}{2}x_0^2\right) + \frac{F_R + R_Z}{3} \\ & + \frac{-4K_G}{L_2\cos\theta\left[M(1-\eta)K_m + H_l K_l\right]\tan\alpha}\left[\frac{\sin\theta}{4}\left(L_2^4\cos^4\theta - x_0^4\right)\right. \\ & \left. - \frac{1}{3}(L_2\sin\theta + h_\perp)\left(L_2^3\cos^3\theta - x_0^3\right) + \frac{h_\perp L_2}{2}\left(L_2^2\cos^2\theta - x_0^2\right)\right] \\ & - \frac{-2f_M}{\tan\alpha}\left(\frac{1}{2}x_0^2 - L_2x_0\right) - \frac{-2K_G}{\left[M(1-\eta)K_m + H_l K_l\right]\tan\alpha}\left[\frac{\sin\theta}{3}\left(L_2^3\cos^3\theta - x_0^3\right)\right. \\ & \left. - \frac{1}{2}(L_2\sin\theta + h_\perp)\left(L_2^2\cos^2\theta - x_0^2\right) + h_\perp L_2(L_2\cos\theta - x_0)\right] \end{aligned} \tag{7}$$

Considering the impact of water immersion on the friction coefficient at the hinged end between the key block B and A, we introduce the friction angle of the rock block φ'. To prevent sliding instability, the following condition needs to be satisfied:

$$T_{AB}tan\varphi' \geqslant R_{AB}. \tag{8}$$

The ratio of the friction force between the key block A and B to the shear force R_{AB} of the arcuate triangular block structure is defined as the sliding stability coefficient K_1.

$$K_1 = \frac{T_{AB}tan\varphi'}{R_{AB}}. \tag{9}$$

As shown in Fig. 9, after the roadway is excavated, under conditions of weak water infiltration, if $K_1 < 0$, the combined support force provided by the coal body and fallen gangue to the arcuate triangular block exceeds the sum of the weight of the arcuate triangular block and the overlying weak rock layer, as well as the shear forces exerted by the adjacent front and rear rock blocks C on the arcuate triangular block. In such cases, the arcuate triangular block will not undergo slip instability after the roadway excavation. However, in the case of increasing water immersion, the reinforcing effect of the mudstone in the immediate roof and the coal body on the stability of the overlying key blocks is notably reduced. At this point, extra frictional resistance from block A acting on block B is necessary to ensure the stability of the overlying rock layers, at this time $K_1 > 1$ ensuring that the arcuate triangular block does not undergo slip instability. Under the action of continuous water immersion, T_{AB} is further weakened, causing the friction force between key blocks A and B to be less than the shear force R_{AB} of the arcuate triangular block structure. In such cases, where $0 < K_1 < 1$, the arcuate triangular block undergoes slip instability.

Simulation study of the roadway in the immersion softening area

Based on a thorough understanding of the stability of the triangular plate structure in the overlying rock, this section examines the hinge instability characteristics of the overlying rock structure following the weakening of mudstone through Similarity simulation experiments. Additionally, it analyzes the distribution and evolution characteristics of the goaf-roadway surrounding rock stress field under immersion conditions using numerical simulation experiments.

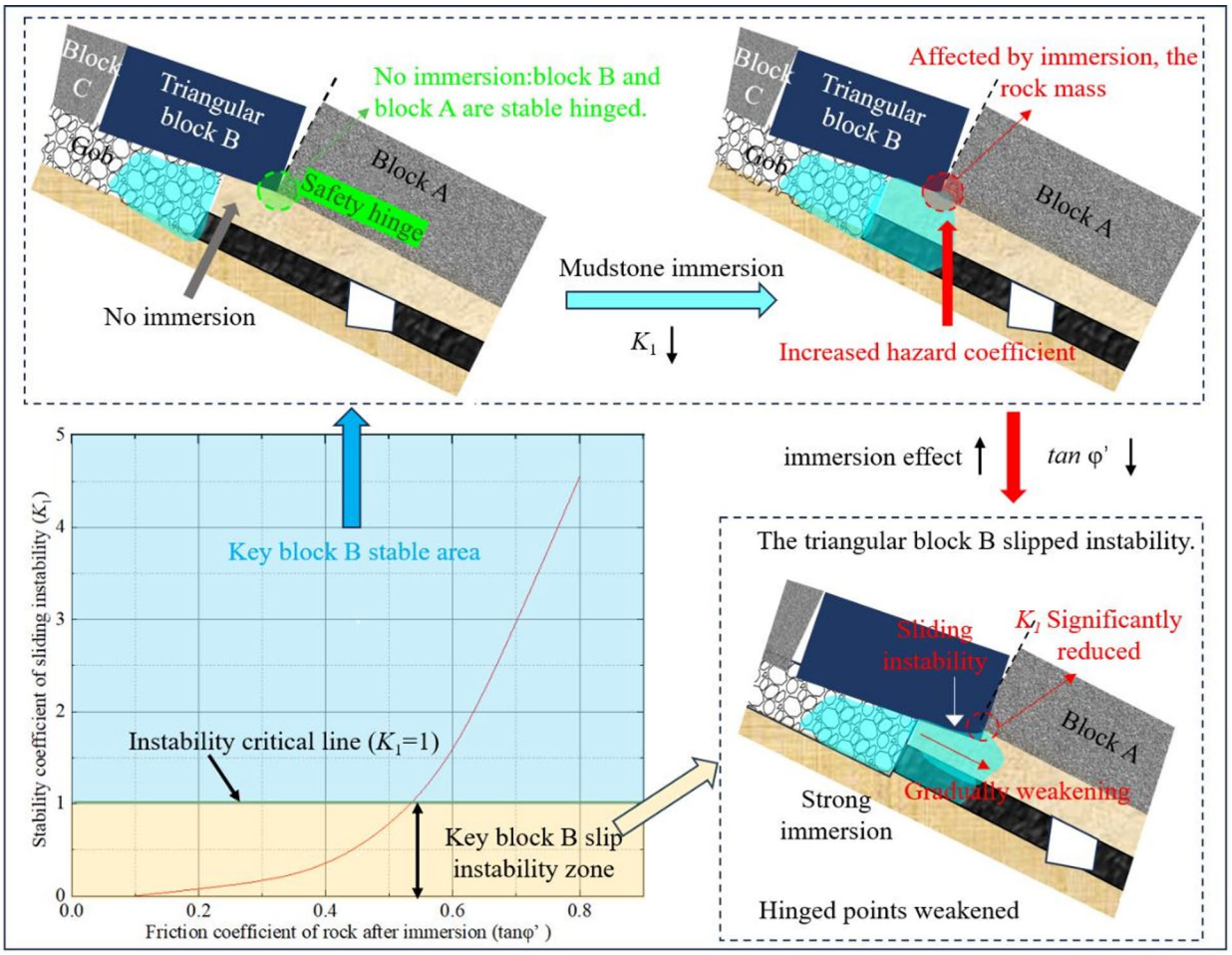

Fig. 9. Trend analysis diagram for sliding stability of key triangular block B.

Similarity simulation experiment

Based on the site engineering conditions and characteristics of the inclined coal seam under water immersion, the following key considerations were addressed during the design phase of the similarity simulation experiment: (1) The material ratio for the coal and rock layers was based on laboratory analysis results of the original rock samples. (2) The volume of materials required for laying the inclined coal and rock layers was specified in advance. (3) After excavation, water was injected uniformly and slowly through a hose directed toward the goaf area. (4) The water injection volume was designed proportionally according to the water content of rock samples measured in laboratory tests. (5) Combined with laboratory water immersion experiment, reasonable soft water-blocking layer is set at the joint of goaf and coal pillar area and direct bottom, in order to match the main water-immersion influence area on site.

Figure 10a and b illustrate the specific experimental arrangements.

Stage 1: before water immersion

In Fig. 10c, during the excavation of the 110,304 return-air roadway, the basic roof and coal pillar area maintained good integrity. In Fig. 10d, the advancement of the 110302WF caused the gob-side-entry-roadway's roof to be suspended, and stress concentration occurred in the coal pillar area and its roof, which eventually led to the breaking of the basic top key layer in the area above the coal pillar, and the fracture line was located 6 m deep into the coal pillar area. The original protective coal pillar width was 16 m, leaving an unaffected 10-meter area as a safety margin beyond the fracture line. At this point, the stability of the overburden key structure at this time belongs to the stable hinge described in the theoretical analysis part.

As the gangue in the goaf is gradually compacted, the cracks in the basic roof become more obvious.

In Fig. 10e, due to the influence of goaf, the water-conducting fissures between the 110302WF and the upper water-bearing zone increase. Based on the on-site hydrogeological report, it is simulated that sufficient water flows into the goaf along the cracks and gradually diffuses and infiltrates along the inclined coal and rock layers.

Stage 2: under the effect of water immersion

The water immersion causes the mudstone layer at the roof of the coal pillar area to show significant mudification, as shown in Fig. 10f.

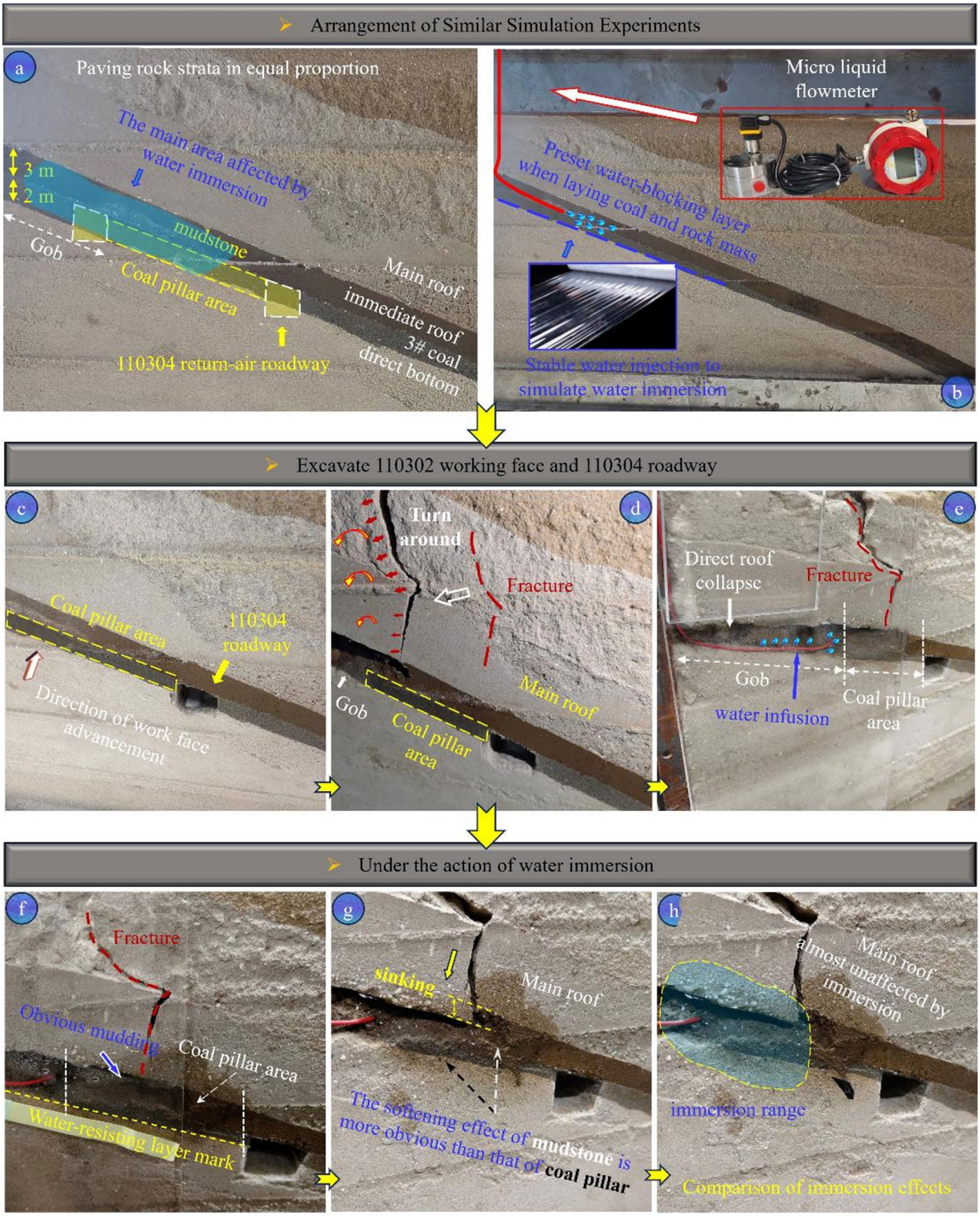

Fig. 10. Similar simulation experiment.

In Fig. 10g, water immersion causes the bearing capacity of the mudstone layer at the roof of the coal pillar area to decrease significantly, and the key blocks of the overburden rock sink significantly, which belongs to the hinged instability of the key blocks after water immersion in the theoretical analysis part.

In Fig. 10h, the softening effect caused by water immersion has a particularly significant impact on the mudstone layer, while the siltstone and the coal pillar remain relatively intact. This is consistent with the laboratory test part and theoretical analysis. This also further proves that the softening of mudstone by water

immersion is the key to the large deformation and damage of the surrounding rock along the goaf in the water-softened area of the inclined rock layer.

Numerical simulation study on the evolution of the stress field in the surrounding rock of the Goaf roadway under the influence of water immersion

The similar simulation above demonstrated the hinge instability characteristics of the overlying rock structure following mudstone weakening. In this section, the stress field distribution and evolution characteristics of the roadway under different degrees of water weakening and different water immersion ranges are studied through numerical simulation experiments, taking support pressure and deviatoric stress as indicators, so as to facilitate the subsequent proposal of a scientific and reasonable surrounding rock control method suitable for roadways along the goaf softening zone under modified geological conditions.

Experimental scheme and model design

The softening and collapse of the mudstone on the direct roof of the roadway after water immersion has a significantly stronger weakening effect on strength than that of the coal seam and siltstone. Therefore, the difference in the influence of water immersion is mainly manifested in the difference in the degree of mudstone weakening and the range of water immersion:

As shown in Fig. 11, In the experiment, the mudstone strength reduction coefficients $S_1 = 0.8$, $S_2 = 0.5$, and $S_3 = 0.2$ were set to simulate the mechanical properties and strength changes of the direct roof mudstone under different softening degrees;

The direct roof mudstone have different water immersion ranges, and the degree of weakening after water immersion is also different. The water immersion range of the direct roof mudstone in the coal pillar area is set to 2 m, 4 m, 6 m, 8 m, and 10 m respectively;

At the same time, the surrounding rock stress field of the roadway after the 110302WF was mined under no water immersion conditions was set as the control group.

The main parameters of the numerical model are length × height × width = 180 m × 150 m × 100 m, and the corresponding parameters are set according to the rock strength test results in the research mining area.

Evolution of the surrounding rock's stress field under the softening of direct roof mudstone due to water immersion

In order to accurately grasp the development law of deformation and failure of the roadway surrounding rock under water immersion, the stress field evolution characteristics of roadway deformation are explored with support pressure and deviatoric stress as research indicators. The figure below intuitively reflects the evolution law of support pressure of surrounding rock that only directl roof subjected to water immersion.

When the range of water immersion is controlled to 10 m, the distribution pattern of abutment stress field under different degrees of immersion-induced weakening is observed (see Fig. 12).

As the degree of water immersion deepens, the strength of the mudstone continuously weakens, and the degree of stress concentration significantly increases. Under non-weakening conditions, the abutment stress in the coal pillar area does not form a strong stress concentration. However, as the strength of the mudstone gradually decreases, the peak abutment stress increases and gradually approaches the roadway ribs, indicating that the weakening of the mudstone reduces the bearing capacity of the coal-rock mass, leading to a decrease in roadway stability.

At a low weakening degree (S_1), the stress concentration zones around the roadway remain unconnected, and the coal-rock mass still possesses considerable bearing capacity. However, when the weakening degree reaches

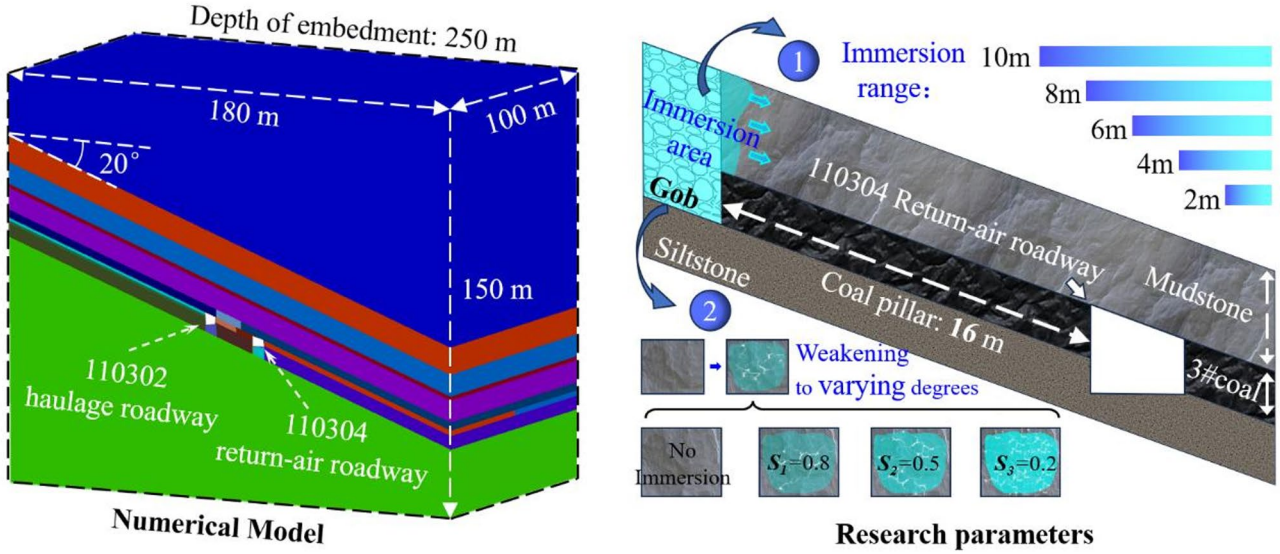

Fig. 11. Establishment of the numerical model and experimental scheme.

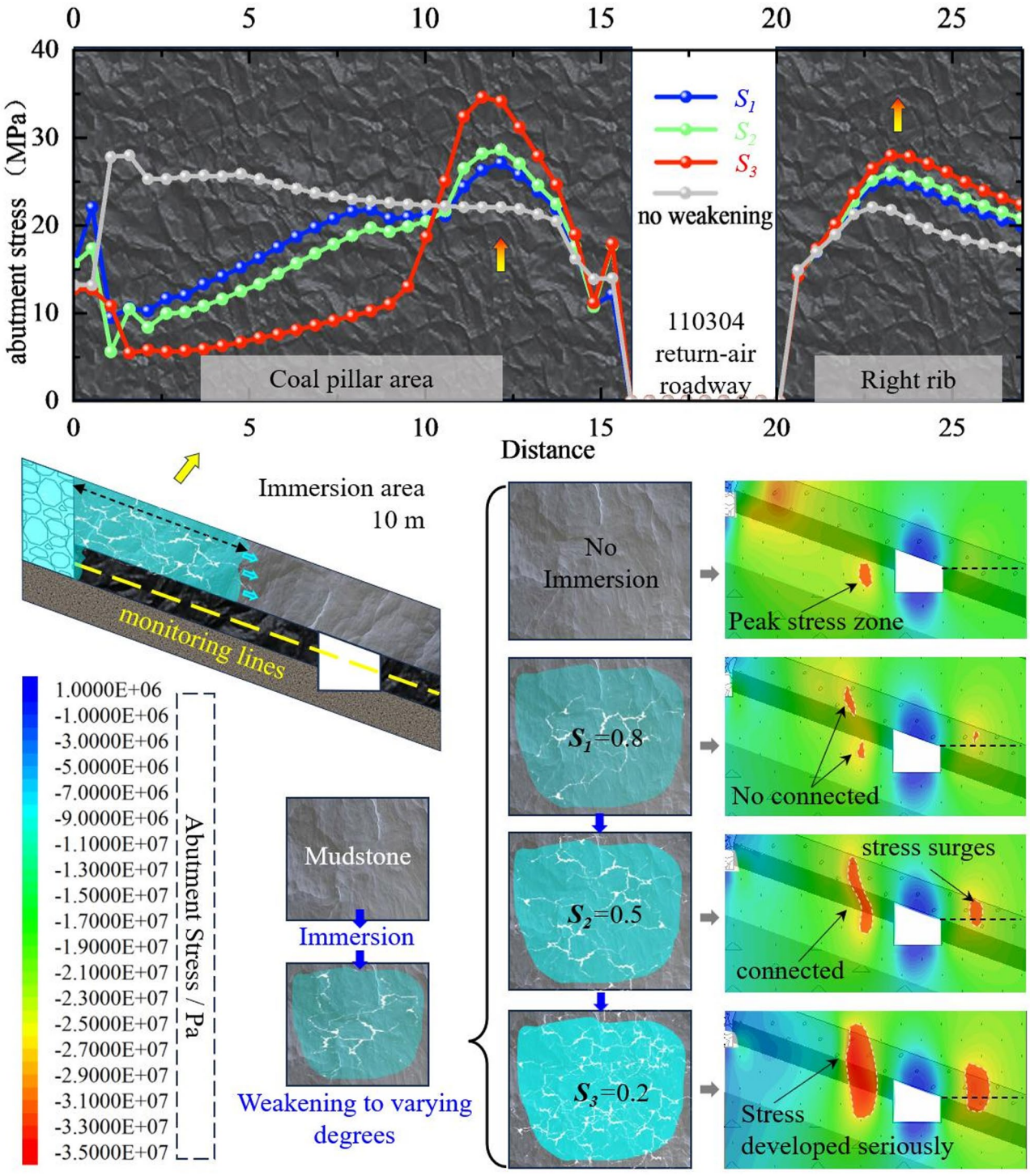

Fig. 12. Evolution of the abutment stress field in the surrounding rock under different degrees of mudstone water immersion.

50% (S_2), the stress concentration area in the coal pillar rib begins to connect and gradually expands. Under strong water immersion (S_3), the high-stress regions in the shallow roadway-surrounding-rock significantly expand, and the surrounding rock shows signs of severe damage.

This change is primarily due to the reduction in mudstone strength in the water-immersed region, which weakens the bearing capacity, increases the extent of low-stress areas, and causes high stress to be transferred toward the roadway ribs, significantly increasing the risk of failure of the roadway.

As shown in Fig. 13, the advancement of peak stress is positively correlated with the extent of water immersion in the direct top mudstone. However, the evolution of the support stress field in the two sides of the protected

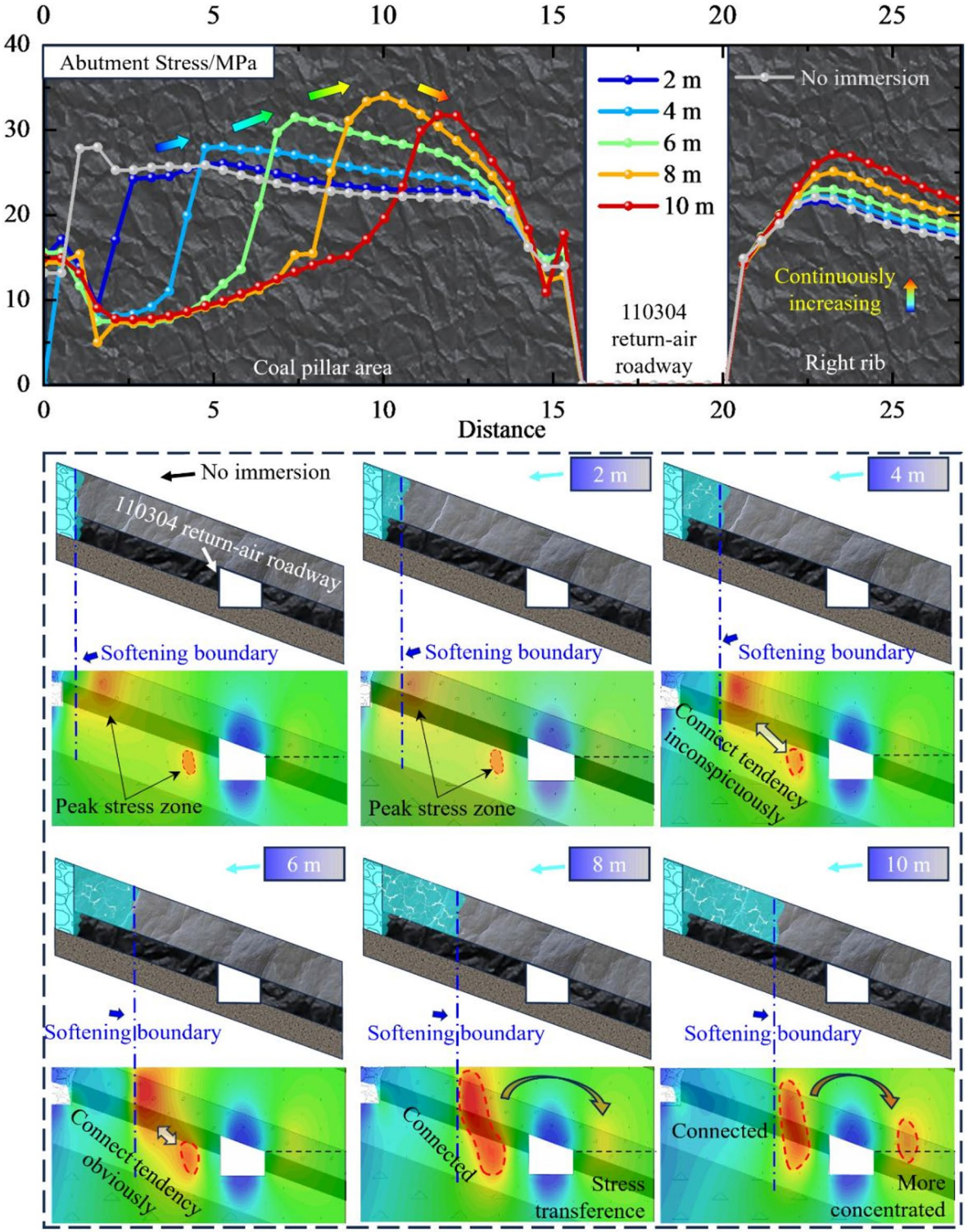

Fig. 13. Evolution of the surrounding rock abutment stress field under different ranges of mudstone water immersion.

roadway exhibits significant differences. As the range of water immersion expands, the high stress area and peak intensity in the coal pillar side first increase and then decrease, while the right side continues to increase.

Figure 14 presents the distribution and evolution of the deviatoric stress field in the surrounding rock under the influence of water immersion, considering different variables such as immersion range and mudstone strength degradation. Analyzing the changes in deviatoric stress under various conditions helps to understand the impact of water immersion on surrounding rock stability.

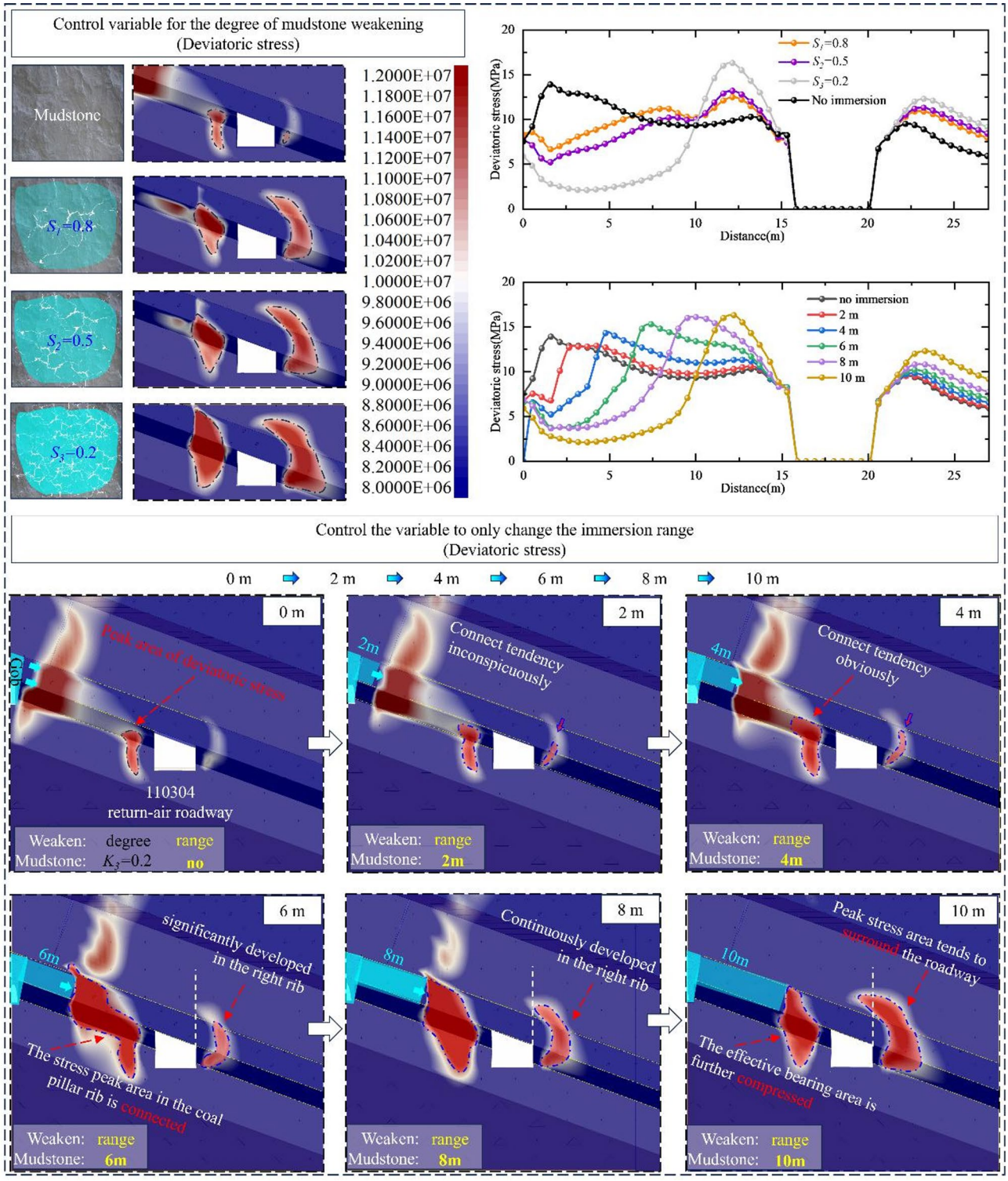

Fig. 14. Distribution and evolution of the deviatoric stress field in the surrounding rock under different water immersion impacts on the direct roof mudstone.

As the immersion range increases or the mudstone strength weakens further, the peak deviatoric stress gradually concentrates toward the coal pillar and roadway edges. This trend indicates that water immersion-induced mudstone weakening exacerbates local stress concentration, increasing the risk of surrounding rock failure in these regions.

Under conditions with smaller immersion ranges or lower weakening degrees (immersion range < 4 m), the high-stress areas of the deviatoric stress field are confined to the roadway's peripheral region, and the surrounding rock's bearing capacity remains relatively stable. However, as the immersion range increases

(immersion range > 6 m), the high-stress area gradually expands and penetrates deeper into the surrounding rock, forming a broader stress concentration zone. This expansion indicates that the impact of water immersion intensifies, increasing the likelihood of instability over a larger area in the roadway.

When the deviatoric stress field connects over a larger range (immersion range ≥ 8 m), the low-strength areas within the surrounding rock link to the high-stress zones, forming potential failure pathways. This connectivity further decreases the overall stability of the roadway. Additionally, as stress shifts from the weakened zones to the roadway sides, the peak stress on the non-coal pillar side of the roadway increases more rapidly, and the peak area expands significantly. This further complicates the difficulty of controlling roadway deformation.

In conclusion, the evolution of the deviatoric stress field under water immersion indicates that controlling the immersion range and mudstone weakening degree is crucial for maintaining the long-term stability of the roadway surrounding rock. The results of this study provide a theoretical basis for roadway support design in water-saturated environments.

Asymmetric large deformation control technology and field monitoring for water-immersed goaf-side roadways

Design of roadway support scheme in water-soaked and softened areas

In the return-air roadway of the 110304WF, the roof support adopts anchor bolts with specifications of φ20 mm × 2200 mm (spacing of 800 mm × 800 mm, 6 per row) and anchor cables of 21.8 mm × 7300 mm (spacing of 1200 mm × 800 mm, 3 per row). The support for the coal pillar side and solid coal side both use φ20 mm × 2200 mm anchor bolts (spacing of 800 mm × 800 mm, 4 per row) and 21.8 mm × 6300 mm anchor cables. The spacing for the coal pillar side anchor cables is 800 mm × 1600 mm (3 per row), while the spacing for the solid coal side anchor cables is 1200 mm × 800 mm (2 per row). All anchor cable trays are 300 mm × 300 mm × 14 mm pallets, as shown in Fig. 15.

In response to the failure characteristics of the immediate roof mudstone under water softening, a targeted combined support measure has been designed. Based on high-strength anchor bolts and cable support systems, we propose a combined water control scheme of 'grouting-based water isolation + pipeline drainage.' This approach addresses the causes of large deformations in mining roadways, with the technical framework illustrated in Fig. 16 (created using PowerPoint Version 2506).

Due to the large amount of water inflow in the goaf, the destruction of the mudstone roof is difficult to control. To prevent damage without affecting the integrity of the coal pillar, two rows of drainage pipes were designed and drilled into the coal pillar side to guide the water level and reduce water inflow. The upper layer drainage pipes are spaced 20 m apart, while the lower layer drainage pipes are spaced 10 m apart, continuously improving the water infiltration environment in the coal pillar mudstone roof.

In the key bearing areas of the mudstone layer, 30-degree angle grouting anchor cables were designed. The grouting process uses two types of grout materials, Marisite and P.042.5R, alternately. The spacing of the grouting anchor cables is 16 m. The modified mudstone significantly improves in strength and water isolation capacity, effectively preventing further water infiltration into the coal pillar.

Traditional support for goaf roadways typically focuses on the side of the roadway near the coal pillar. However, the stress field evolution in the surrounding rock during water immersion shows that, while the stress concentration in the coal pillar side is relatively high, the stress concentration increase on the work face side under strong water immersion conditions is also significant. Therefore, in addition to asymmetric anchor cable support on the coal pillar side, a combined shelf-cable support system has been designed. On the basis of the original shelf support, a row of I-beams is inserted between every two rows of anchor cables. The I-beams are connected to the original anchor cables with steel ropes, forming a systematic support network that significantly enhances the strength of the roadway support, as shown in Fig. 17 (created using PowerPoint Version 2506).

Field monitoring and feedback

To thoroughly assess the operational status of the roadway support structure under the proposed design scheme and accurately determine the control effect of the surrounding rock under targeted support, displacement monitoring stations were set up after the roadway was expanded and renovated. The displacement of the roof, floor, and both sidewalls of the roadway was continuously monitored using a cross-point method, and displacement-time curves were plotted.

As shown in Fig. 18, the deformation of the surrounding rock gradually increased over time. In the first 15 days, the deformation was relatively small, remaining at a low development rate. Between 15 and 30 days, the deformation rate of the surrounding rock significantly accelerated, with a noticeable increase in displacement, indicating that the surrounding rock was in a more active deformation phase during this period. After 34 days, the deformation of the surrounding rock stabilized and entered a steady phase. The monitoring results showed that the maximum displacement values for the roof and floor, coal pillar side displacement, and solid coal side displacement were 178 mm, 99 mm, and 89 mm, respectively, all within a controllable range. The drilling peep results in the figure also reflect that the the grouting isolation and pipe drainage in the support scheme are effective, and the surface integrity of the roadway remains well-maintained after shotcreting.

This indicates that the roadway support scheme designed in this study demonstrated good applicability and effectiveness in controlling surrounding rock deformation, meeting the surrounding rock control requirements well.

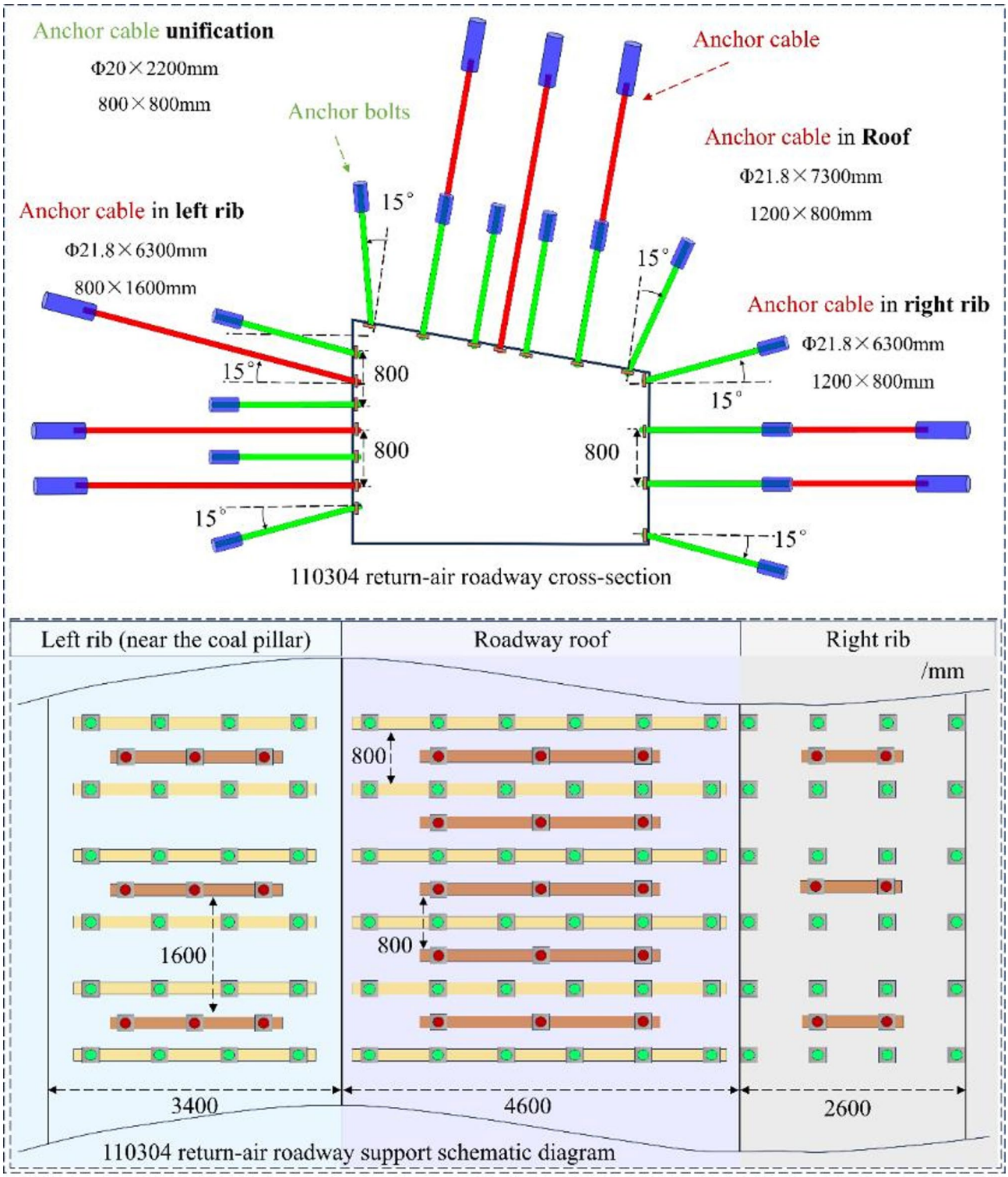

Fig. 15. Schematic diagram of bolt and cable support.

Conclusions

(1) The direct roof mudstone contains a large amount of clay minerals, such as kaolinite(30%), which exhibit significant expansion and weakening characteristics under water immersion. This considerably reduces the strength and integrity of the direct roof mudstone, while the coal body and the sandstone in the roof and floor are negligibly affected. The strength reduction and deterioration in load-bearing capacity of the direct

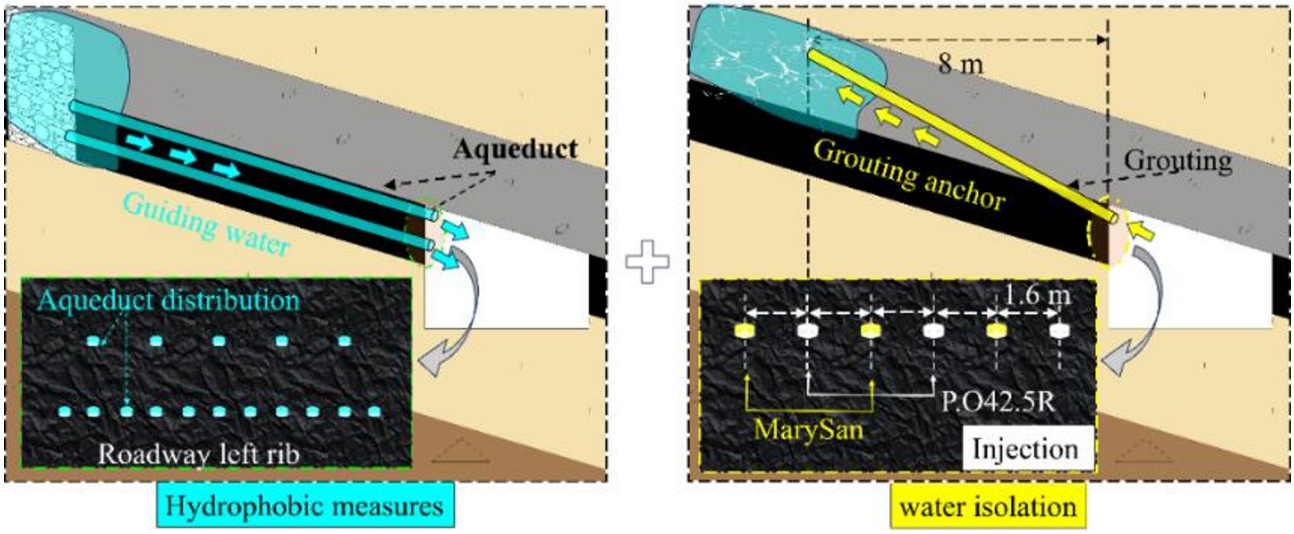

Fig. 16. Grouting water isolation-pipeline water diversion combined support.

roof mudstone after water immersion softening are the fundamental causes of large deformations in the roadway.

(2) By introducing the weakened friction angle of rock blocks, φ', and the sliding stability coefficient, K_1, under the influence of water immersion, a stability evaluation system for the key block of the basic roof above the goaf roadway under water immersion is established.

(3) The similar simulation experiment showed that the strength of the mudstone roof above the coal pillar significantly decreases after water immersion, causing further instability in the previously hinged-stable key block of the basic roof, thereby threatening the safety of the underlying roadway. This observation confirms the validity of the stability evaluation system for the key block of the basic roof in the goaf roadway under water immersion.

(4) Numerical simulations analyzed the stress distribution and evolution pattern of the surrounding rock in the goaf roadway of an inclined coal seam under water immersion. As the water immersion effect on the mudstone roof intensifies, the peak stress zones of the coal pillar and the roadway sidewall begin to connect. Under high-intensity water immersion, the rate of stress increase in the solid coal sidewall accelerates, and the peak stress zone area expands sharply, enveloping the roadway. Under the 16 m coal pillar condition in this study, the peak stress zone becomes connected when weakening exceeds 6 m, and when it surpasses 8 m, the peak stress zone on the right sidewall rapidly expands, extending toward the roof and floor.

(5) Based on the above findings, an asymmetric large deformation support control technology—"grouting and drainage + combined shed and cable support"—was proposed for water-immersed goaf roadways. On-site monitoring feedback shows that the tunnel deformation is controllable, the surrounding rock integrity is good, and the support method is effective. It has important significance for other similar working conditions. Field monitoring feedback indicated that the roadway deformation was controllable, the surrounding rock maintained good integrity, and the support method was effective, offering valuable insights for similar conditions.

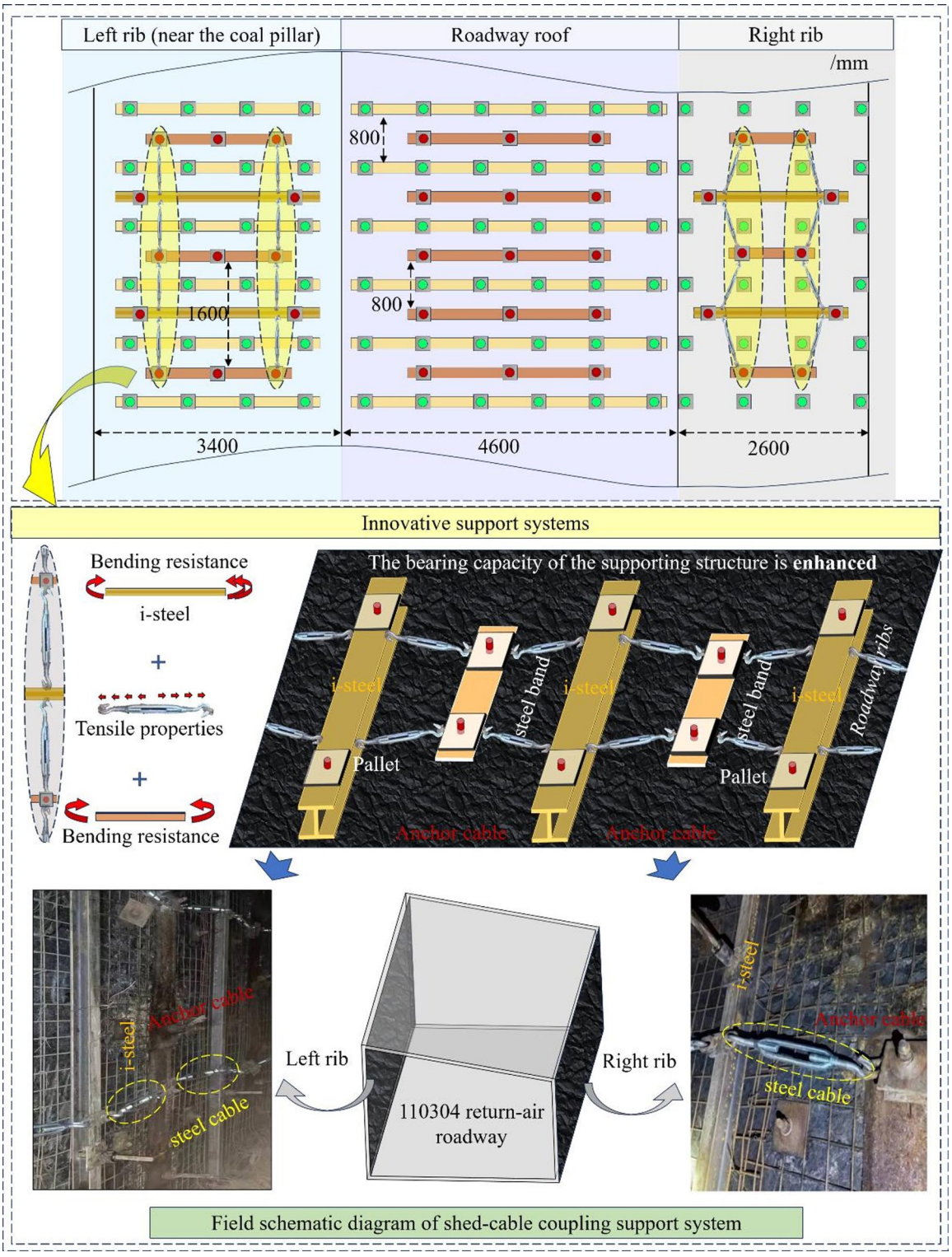

Fig. 17. Principle and application of shed-cable coupling support.

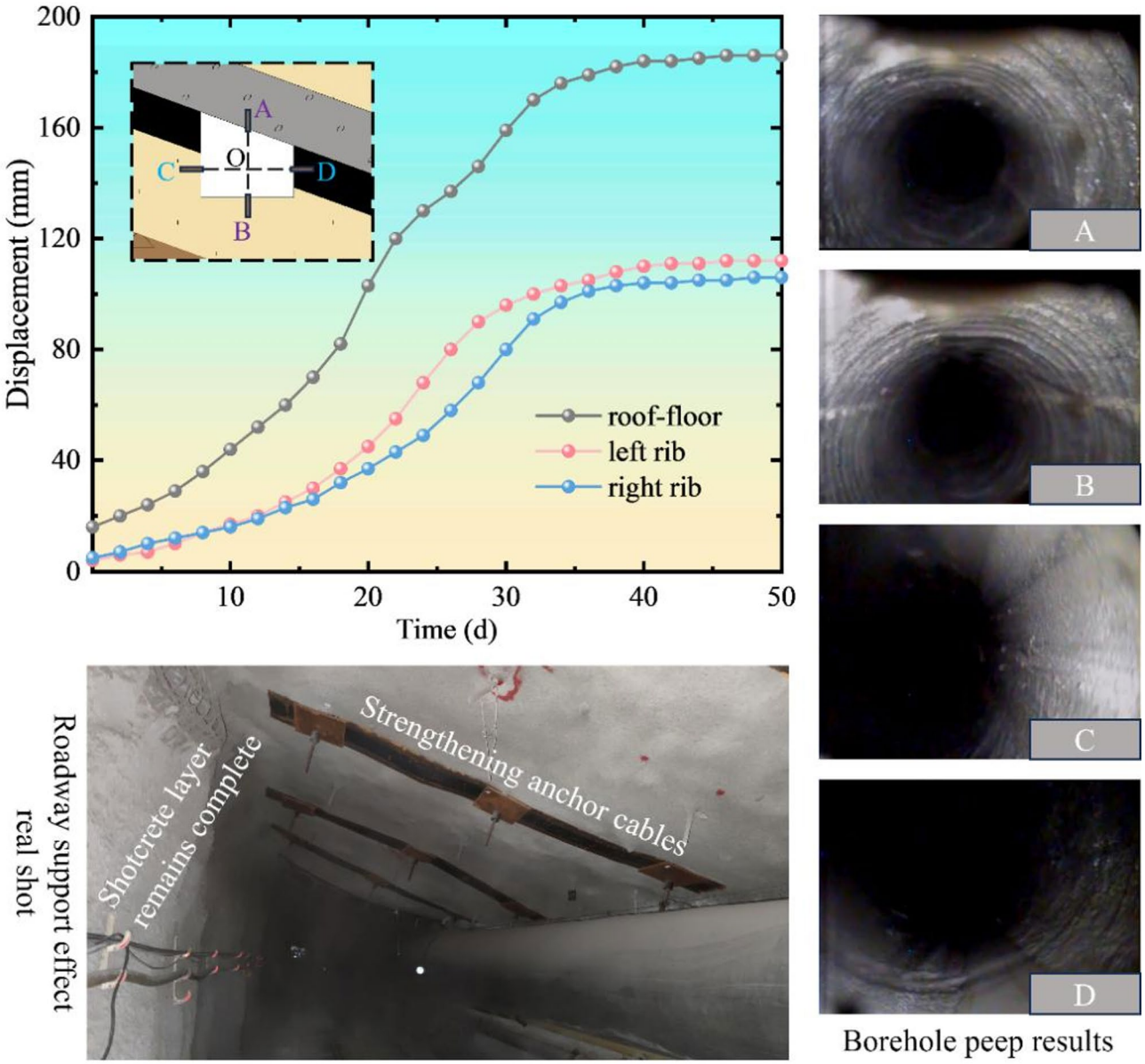

Fig. 18. Field monitoring results.

Data availability

All data generated or analysed during this study are included in this published article.

Received: 23 December 2024; Accepted: 14 July 2025
Published online: 22 July 2025

References

1. Ji, J. S., Li, Z. H., Yang, K. & Zhou, G. H. Research on formation mechanism and evolution pattern of bed separation zone during repeated mining in multiple coal seams. *Geofluids* (2022).
2. Chen, A., Li, X. B. & Liu, X. S. Relief-retaining control technology of floor heave in mining roadway with soft rock: A case study. *Adv. Civ. Eng.* (2021).
3. Wu, Y. P., Wu, X. M. & Chen, Z. Z. Comprehensive analysis of large trapezoidal section workings' stability in broken rock mass. *Rock Mech. Achiev. Ambit.*, 51–56 (2012).
4. Chen, D. D., Jiang, Z. S. & Ma, X.Evolution law and engineering application on main stress difference for a novel stress relief technology in two ribs on deep coal roadway. *J. Cent. South Univ.* **30** (7), 2266–2283 (2023).
5. Ma, L. J., Zhao, B. F., Wang, H. & Gao, Y. Analysis of Spatial differences in permeability based on sedimentary and structural features of the sandstone aquifer overlying coal seams in Western China. *Mine Water Environ.* **39** (2), 229–241 (2020).
6. Dong, Y. et al. Fine detection on water abundance of sandstone by joint inversion of seismic and CSAMT: a case study in the Western Ordos basin, China. *Acta Geophys.* **70** (5), 2045–2056 (2022).

7. Xu, H. C., Lai, X. P., Zhang, S. & Zhang, Y. Multiscale intelligent inversion of water-conducting fractured zone in coal mine based on elastic modulus calibration rate response and its application: A case study of Ningdong mining area. *Lithosphere* (2021).
8. Xu, X., Wang, X. Z. & Li, Y. Z. Prediction of the height of water flowing fractured zone based on the MPSO-BP neural network model. *Math. Probl. Eng.* (2022).
9. Zeng, Y. F., Yang, D. H. & Wu, Q. Mechanism of instantaneous High-Strength Sand-Water inrush in steeply inclined mining of soft coal seam under disturbed Rock-Soil overburden. *Lithosphere* **2024** (3) (2024).
10. Kong, D. Z., Xiong, Y. & Cheng, Z. B. Stability analysis of coal face based on coal face-support-roof system in steeply inclined coal seam. *Geomech. Eng.* **25** (3), 233–243 (2021).
11. Wang, H., Qin, Y., Wang, H. B. & Liu, X. C. Process of overburden failure in steeply inclined multi-seam mining: insights from physical modelling. *R. Soc. Open. Sci.*, **8** (5) (2021).
12. Ma, F. H., Sun, L. & Li, D. Numerical simulation analysis of covering rock strata as mining steep-inclined coal seam under fault movement. *Trans. Nonferrous Met. Soc. China*. **21**, S556–S561 (2012).
13. Sun, Y. J., Zuo, J. P. & Karakus, M. A new theoretical method to predict strata movement and surface subsidence due to inclined coal seam mining. *Rock Mech. Rock Eng.* **54** (6), 2723–2740 (2021).
14. Asadi, A., Shahriar, K., Goshtasbi, K. & Najm, K. Development of a new mathematical model for prediction of surface subsidence due to inclined coal-seam mining. *J. South. Afr. Inst. Min. Metallurg.* **105** (1), 15–20 (2005).
15. Asadi, A., Shakhriar, K. & Goshtasbi, K. Profiling function for surface subsidence prediction in mining inclined coal seams. *J. Min. Sci.* **40** (2), 142–146 (2004).
16. Li, X. S., Wang, Y. M., Hu, Y. J., Zhou, C. B. & Zhang, H. Numerical investigation on stratum and surface deformation in underground phosphorite mining under different mining methods. *Front. Earth Sci.* **10** (2022).
17. Yin, Y. C., Zhao, T. B., Zhang, Y. B., Tan, Y. L. & Qiu, Y. An innovative method for placement of gangue backfilling material in steep underground coal mines. *Minerals* **9** (2) (2019).
18. Chen, D. D., Jiang, Z. S., Xie, S. R. Mechanism and key parameters of stress load-off by innovative asymmetric hole-constructing on the two sides of deep roadway. *Int. J. Coal Sci. Technol.* **10**, 82 (2023).
19. Yang, W. M., Li, L. C., Li, X. J. & Wang, L. G. Water outbursts in underground mining with steeply dipping coal seams: numerical simulations based on a mining case. *Eur. J. Environ. Civil Eng.* **18** (5), 511–535 (2014).
20. Wang, Y. & Haoran, L. Experimental study on the compression and shear deformation evolution of coal pillar dam samples. *Sci. Rep.* **14** (1), 1–10 (2024).
21. He, S. Q., Song, D. Z. & Li, Z. L. Precursor of Spatio-temporal evolution law of MS and AE activities for rock burst warning in steeply inclined and extremely Thick coal seams under caving mining conditions. *Rock Mech. Rock Eng.* **52** (7), 2415–2435 (2019).
22. He, S. Q., Song, D. Z., He, X. Q. & Chen, J. Q. Coupled mechanism of compression and prying-induced rock burst in steeply inclined coal seams and principles for its prevention. *Tunn. Undergr. Space Technol.* **98**, 1–10 (2020).
23. Lai, X. P., Xu, H. C. & Shan, P. F. Research on the mechanism of rockburst induced by mined coal-rock linkage of sharply inclined coal seams. *Int. J. Minerals Metall. Mater.* **31** (5), 929–942 (2024).
24. Das, A. J., Mandal, P. K., Paul, P. S., Sinha, R. K. & Tewari, S. Assessment of the strength of inclined coal pillars through numerical modelling based on the ubiquitous joint model. *Rock Mech. Rock Eng.* **52** (10), 3691–3717 (2019).
25. Das, A. J., Mandal, P. K., Paul, P. S. & Sinha, R. K. Generalised analytical models for the strength of the inclined as well as the flat coal pillars using rock mass failure criterion. *Rock Mech. Rock Eng.* **52** (10), 3921–3946 (2019).
26. Das, A. J., Paul, P. S., Mandal, P. K., Kumar, R. & Tewari, S. Investigation of failure mechanism of inclined coal pillars: numerical modelling and tensorial statistical analysis with field validations. *Rock Mech. Rock Eng.* **54** (6), 3263–3289 (2021).
27. Ning, J. G., Wang, J., Bu, T. T., Hu, S. C. & Liu, X. S. An innovative support structure for Gob-Side entry retention in steep coal seam mining. *Minerals* **7** (5) (2017).
28. Wu, G. J. et al. An anchorage experimental study on supporting a roadway in steeply inclined geological formations. *Tunn. Undergr. Space Technol.* **82**, 125–134 (2018).
29. Chen, D. X., Sun, C. & Wang, L. G. Collapse behavior and control of hard roofs in steeply inclined coal seams. *Bull. Eng. Geol. Environ.* **80** (2), 1489–1505 (2021).
30. Xiong, X. Y., Dai, J., Ouyang, Y. B. & Shen, P. Experimental analysis of control technology and deformation failure mechanism of inclined coal seam roadway using non-contact DIC technique. *Sci. Rep.* **11** (1) (2021).
31. Chen, G. B. et al. Damage effect and deterioration mechanism of mechanical properties of fractured Coal-Rock combined body under Water-Rock interaction. *Rock Mech. Rock Eng.* **58** (1), 513–537 (2025).
32. Dudek, M. & Tajdus, K. FEM for prediction of surface deformations induced by flooding of steeply inclined mining seams. *Geomech. Energy Environ.* **28** (2021).
33. Wu, L. Y., Bai, H. B. & Ma, D. Prediction and prevention of water inrush hazards from bed separation space. *Mine Water Environ.* **40** (3), 657–670 (2021).
34. Shan, P. F. & Lai, X. P. Numerical simulation of the Fluid-Solid coupling process during the failure of a fractured Coal-Rock mass based on the regional geostress. *Transp. Porous Media*. **124** (3), 1061–1079 (2018).
35. Xu, Y. C., Luo, Y. Q., Li, J. H., Li, K. Q. & Cao, X. C. Water and sand inrush during mining under Thick unconsolidated layers and thin bedrock in the Zhaogu 1 coal mine, China. *Mine Water Environ.* **37** (2), 336–345 (2018).
36. Wang, W. Q., Li, Z. H., Du, F., Cao, Z. Z. & Li, G. S. Study of roof water inrush control technology and water resources utilization during coal mining in a karst area. *Mine Water Environ.* **42** (4), 546–559 (2023).
37. Cao, Z. Z., Zhang, S. Y., Xue, Y. & Wang, Z. X. Disaster-Causing mechanism of spalling rock burst based on folding catastrophe model in coal mine. *Rock Mech. Rock Eng.* **1**, 1–14 (2025).

Acknowledgements

This research was supported with funding awarded from the National Natural Science Foundation of China (Grant No. 52004286, 52374149).

Author contributions

CY.T. was responsible for the initial idea and conceptual framework of the research project. DD.C., SK.X., ZX.Z. and WK.Z. were involved in the organization, cleaning, and preparation of the research data. CY.T. secured the necessary funding for the research project. CY.T. and ZJ.L. conducted the research investigation, including designing and executing experiments or studies to address the research question. CY.T. a1nd ZJ.L. developed and refined the research methodology, ensuring it was appropriate and rigorous for addressing the research objectives. ZJ.L., JC.C. and XY.Y. were responsible for selecting, implementing, and utilizing software tools necessary for data analysis and research execution. ZJ.L. and JC.C. conducted the laboratory tests and experiments required for the research. ZJ.L. and JC.C. were primarily responsible for drafting the initial version of the manuscript, incorporating the research findings and analysis. CY.T. reviewed and edited the manuscript, providing critical feedback and ensuring that the content was clear, accurate, and met the required standards for publica-

tion. Figures 7 and 8, and 9 were created by Jingchen Chang; Figs. 16 and 17 were created by Zijian Li. All figures were drawn by the research team. The software used for drawing is Microsoft PowerPoint 2019 version 2504. All authors reviewed the manuscript.

Declarations

Competing interests

The authors declare no competing interests.

Additional information

Correspondence and requests for materials should be addressed to D.C.

Reprints and permissions information is available at www.nature.com/reprints.

Publisher's note Springer Nature remains neutral with regard to jurisdictional claims in published maps and institutional affiliations.